Desalination and Water Treatment
www.deswater.com

doi:10.5004/dwt.2017.20831

79 (2017) 204–213
June

Kinetics of photocatalytic mineralization of oxytetracycline and ampicillin using activated carbon supported ZnO/$ZnWO_4$ nanocomposite in simulated wastewater

Pankaj Raizada*, Jyoti Kumari, Pooja Shandilya, Pardeep Singh

School of Chemistry, Faculty of Basic Science, Shoolini University, Solan (Himachal Pradesh) 173212, India, Tel. +91-1792-308000, email: pankajchem1@gmail.com (P. Raizada), jtchemorg@gmail.com (J. Kumari), poojashandil03@gmail.com (P. Shandilya), pardeepchem@gmail.com (P. Singh)

Received 10 November 2016; Accepted 14 April 2017

ABSTRACT

In this work, activated carbon supported ZnO/$ZnWO_4$ nanocomposite (ZnO/$ZnWO_4$/AC) was synthesized successfully using modified hydrothermal method. ZnO/$ZnWO_4$/AC composite was characterized using energy-dispersive X-ray (EDX), Fourier transform infrared spectroscopy (FTIR), scanning electron microscopy (SEM), X-ray diffraction (XRD), and UV-visible(UV-vis) spectral analysis and transmission electron microscopy (TEM). The SEM studies clearly revealed the stacking of ZnO/$ZnWO_4$ over activated carbon. ZnO/$ZnWO_4$/AC had rod like arrangement with variable length from 45 nm to 147 nm and diameter between 26 nm to 36 nm. The photocatalytic efficacy of ZnO/$ZnWO_4$/AC was tested for the synergistic degradation of oxytetracycline (OTC) and ampicillin (AMP) from aqueous phase under solar light. The oxidative antibiotics degradation occurred through hydroxyl radicals. Both antibiotics were completely mineralized under solar light. The power law model was used to understand the kinetics of mineralization process. ZnO/$ZnWO_4$/AC exhibited significant recycle ability due to easier separation and stability in reaction solution.

Keywords: Supported ZnO/$ZnWO_4$; Enhanced-photocatalysis; Antibiotic removal; Power law model; Kinetics

1. Introduction

Antibiotics are used worldwide in pharmaceuticals and personal care products [1,2]. The pharmaceutical pollutants in the aquatic environment pose a major threat due to their bio-reluctant nature. Ampicillin (AMP) and oxytetracycline (OTC) are the most detected pharmaceutical active compounds. AMP is a semi-synthetic penicillin which possesses antimicrobial activity due to beta-lactam ring in its structure [2]. Tetracyclines (TCs) are the important member of antibiotic group that are used for the treatment and prevention of various disease [2]. The various physic-chemical methods such as coagulation, flocculation, carbon adsorption, ultra-filtration, sedimentation, precipitation, membrane separation techniques etc. have already been used previously for waste water treatment. But these conventional methods are incompetent for the complete degradation of organic pollutants into harmless compounds. For example, adsorption process just transfers pollutants form one phase to another and causing secondary pollution [3]. Membrane fouling is major limitation of membrane based filtration processes [4].

Recently, solar light assisted heterogeneous photocatalysis has emerged as most effective technique for the complete removal of aqueous phase pollutants [1]. Heterogeneous photocatalysis involves the oxidative degradation of targeted molecules by generation of highly active free radicals ($OH^{\cdot}$). The hydroxyl radicals with oxidation potential of 2.7 eV degrade organic pollutants CO_2, H_2O and inorganic ions [4]. The metal oxides based semiconductor are emerging as dynamic photocatalysts offering an environmental friendly and vibrant alternative for cleaning water bodies by demineralization of organic and

*Corresponding author.

inorganic contaminants by utilizing solar light [3]. During last decade, ZnO has been used as photocatalyst due to its electronic properties (band gap = 3.37 eV), low cost, high photocatalytic efficiency, chemical stability and non-toxicity [5–8]. $ZnWO_4$ is a ternary photocatalyst having good photocatalytic activity for wastewater treatment. $ZnWO_4$ has been effectively used for the decomposition of salicylicacid [9], decolouration of methyl orange [10], malachite green [11,12] and rhodamine 6G [13]. Zhu et al. investigated visible light activity of graphene-$ZnWO_4$nanocomposites for the photodegradation of methylene blue dye [14]. However, agglomeration and difficult separation of nanoparticles from reaction solution are major bottlenecks associated with bare metal oxide nanoparticles. Secondly, adsorption of aqueous phase pollutants is highly needed for efficient photocatalytic process. The aqueous phase pollutants are poorly adsorbed on the surface bare metal oxides [8]. The supported photocatalysis and coupling of two or more semiconductors have emerged as prominent strategies to over overcome above-mentioned drawbacks of conventional metal oxide photocatalyst [4–6]. Recently, activated carbon has emerged as a most commonly used support/adsorbent in wastewater treatment due to its low cost, large specific surface area and porous structure [6]. Guatam et al. explored photocatalytic activity of graphene sand composite supported $ZnFe_2O_4$ for the mineralization of antibiotics in aqueous phase [15].

The precedent work was focused on the applicability of ZnO/$ZnWO_4$/AC for the degradation of oxytetracycline (OTC) and ampicillin (AMP) from aqueous phase. ZnO/$ZnWO_4$ was prepared and immobilized on activated carbon using simple hydrothermal method. ZnO/$ZnWO_4$/AC was characterized by spectral techniques SEM, TEM, EDX, FTIR, XRD and UV-Vis analysis. The co-operative effect between adsorption and photocatalysis was investigated to optimize the degradation of antibiotics. Power law model was also applied to understand the aspects of long term degradation process. The recyclability of ZnO/$ZnWO_4$/AC catalyst was also tested during degradation process. Lastly, the most plausible mechanism for adsorptional-photocatalytic antibiotic degradation was proposed.

2. Experimental

2.1. Synthesis of ZnO

ZnO was prepared with modification in previously reported work [6]. In a typical synthesis, 0.1 M of zinc nitrate hexahydrate was dissolved in 50 ml of distilled water and sonicated for 30 min to form a homogeneous solution. The pH of solution was adjusted to 9.0 using NaOH (0.5 M). To above solution 0.5 M sodium hydroxide was added and mixture was stirred for 1 h [6]. The ZnO precipitates were filtered and washed with ethanol and doubled is tilled water several times. Finally, the obtained ZnO sample was dried in a vacuum oven at 50°C for 4 h.

2.2. Synthesis of $ZnWO_4$

$ZnWO_4$ composite was prepared using modified hydrothermal method. Briefly, 0.1 M aqueous solution of $[Na_2(WO_4)_2H_2O]$ was prepared by dissolving 1.6 g in 50 ml distilled water. To this solution, 5 mmol of zinc nitrate hexahydrate $[Zn(NO_3)_2{\cdot}6H_2O]$ was added and magnetically stirred for 20 min followed by sonication. The pH of solution was adjusted to 9 using 0.5 M NaOH. After cooling, the precipitates were filtered, washed and dried at 150°C for 1 h. The obtained composites were labelled as $ZnWO_4$ and preserved for further use.

2.3. Synthesis of ZnO/$ZnWO_4$/AC composite

The hydrothermal method was used to synthesize ZnO/$ZnWO_4$/AC composite. Activated carbon powder (1.0 g), and 1.0 g of ZnO were mixed in 100 ml of distilled water. The solution was magnetically stirred for 30 min followed by sonication for 20 min [8]. To this mixture, $Zn(NO_3)_2{\cdot}6H_2O$ (1.5 g) and $Na_2(WO_4)_2H_2O$ (1.5 g) were added with continuous stirring for 30 min. Further, the mixture was sonicated for 1 h. The precipitates were filtered, washed and dried at 200°C for 1 h. The obtained composite was labelled as ZnO/$ZnWO_4$/AC. ZnO/$ZnWO_4$ was prepared using same methodology without the addition of activated carbon support.

$$\begin{aligned} &Na_2WO_4 \cdot 2H_2O + Zn(NO_3)_2 \cdot 6H_2O + AC + ZnO \\ &\quad \rightarrow ZnO / ZnWO_4 / AC + 2NaNO_3 + 8H_2 \end{aligned} \tag{1}$$

Fourier-transform infrared spectra (FTIR) were recorded on Perkin–Elmer spectrometer (Spectrum RX-I). The FESEM micrographs of ZnO/$ZnWO_4$/AC were recorded through model Nava Nano SEM-45(USA). The HRTEM and EDX results were obtained under vacuum conditions using model FP/5022-Tecnai G2 20 S-TWIN (USA). Panalytical's X'Pert Prodiffractrometer was used for powder XRD. The optical absorption analysis was performed using diffuse reflectance spectrophotometer (UV 3600, Shimadzu).

2.4. Photocatalytic and adsorption experiments

The photocatalytic activity of ZnO/$ZnWO_4$/AC was explored in a slurry type (ht. 7.5 cm × dia. 6 cm) enclosed by thermostatic water circulation arrangement (30 ± 0.3°C) [1]. During experiments, slurry composed of antibiotics and ZnO/$ZnWO_4$/AC catalyst suspension was magically stirred with simultaneous exposure to under solar light. For degradation analysis, aliquot (3 mL) was withdrawn and catalyst particles were separated from aliquot [16]. The absorbance of AMP and OTC was observed at 260 and 280 nm, respectively. The solar light intensity was measured by digital lux-meter. The photocatalytic experiments were performed between March to May 2015 (11 am to 2 pm). The chemical oxygen demand (COD) was measured using closed reflux method [1]. The unreacted oxidant was estimated by titrating sample with ferrous ammonium sulphate using ferroin indicator. All the experiments were undertaken in triplicate with errors below 5% and average values were reported. CO_2 measurements were performed using earlier reported methods. The inorganic ions were detected using TDS bench top ion analyser. The removal efficiency was calculated by Eq. (2).

$$\alpha h\nu = B\left(h\nu - E_g\right)^n \tag{2}$$

where C_0 is the initial concentration of sample/COD and C_t/COD is instant concentration of sample/COD. The pH of zero point charge was estimated using previously reported method [1,6].

3. Results and discussion

3.1. Morphological and structural characterization of ZnO/$ZnWO_4$/AC

Figs. 1a,b depict the SEM images of pure AC (a) and ZnO/$ZnWO_4$/AC composites (b) respectively. Fig. 1a reveals the porous nature of activated carbon which facilitate the adsorption of organic/inorganic molecules. These pores exhibited good possibility to entrap the ZnO/$ZnWO_4$/AC particles on its surface. Fig. 1b depicts the non-uniform aggregation of ZnO/$ZnWO_4$ on the surface of activated carbon [17]. EDX pattern of activated carbon and ZnO/$ZnWO_4$/AC composites is presented in Figs. 1c and d. The activated carbon had an elemental composition of carbon (C) and oxygen (O). EDX spectra of activated carbon supported ZnO/$ZnWO_4$/AC nanocomposite confirmed the presence of zinc (Zn), tungstate (W), oxygen (O) and carbon (C) elements (Fig. 1d).

The TEM micrographs and SAED patterns (inset) of ZnO, $ZnWO_4$, ZnO/$ZnWO_4$/AC composites are given in Figs. 2 a–c. Fig. 2a indicates the spherical like shape of ZnO. The SAED micrographs of ZnO had distinguish able diffraction patterns with good crystallinity. TEM analysis of ZnO/$ZnWO_4$ revealed cubic and spherical particles arrangement in an irregular fashion [18]. Fig. 2c depicts the attachment of ZnO/$ZnWO_4$ over the surface activated carbon [16,17]. ZnO/$ZnWO_4$/AC composites displayed more easily distinguishable diffraction patterns with semi-crystalline nature of ZnO/$ZnWO_4$/AC [16–18].

XRD diffractogram of activated carbon is represented in Fig. 3a. The diffraction peaks at 23.89° and 44.00° were due to (002) and (001) planes (JCPDS 36–1451) for activated carbon [19]. Fig. 3b illustrates the XRD spectrum of $ZnWO_4$. The diffraction peaks at the position of 22.206°, 23.061°, 29.430°, 31.65°, 34.43°, 35.95°, 39.4°, 43.14°, 45.30°, 59.18°, 64.56°, and 76.10° were corresponded to (100), (110), (111), (020), (021), (200), (121), (200), (211), (220), (041) and (311) planes. The results of the data matched well with the standard JCPDS file (JCPDS-15-0774) and (JCPDS-82-1691). The XRD difffractogram of ZnO/$ZnWO_4$/AC nanocomposite is shown in Fig. 3c. The semi-crystalline nature of ZnO/$ZnWO_4$/AC nanocomposite was depicted by XRD analysis. The characteristic diffraction peaks at the position of 31.80°, 34.44°, 36.55°, 47.91°, 57.13°, 62.94° and 68.21° were assigned to (100), (002), (110), (211), (102), (103) and (112) planes. These results are in good agreement with the standard JCPDS file (JCPDS 36-1451) and (JCPDS-15-0774) [20,21]. The shift in diffraction peaks was an indicative of ZnO/$ZnWO_4$/AC formation.

FTIR analysis was used to find main functional groups in AC, $ZnWO_4$ and ZnO/$ZnWO_4$/AC (Fig. 4a–c). In activated carbon spectrum, the characteristic peaks of carbon and hydrogen functionalities were observed at 2924 and 2009 cm^{-1}. These peaks were assigned to asymmetric and symmetric C–H stretching vibration of methyl and methylene groups, respectively [22]. The peak at 1516 cm^{-1} was due to OH bending vibration of surface-adsorbed water of

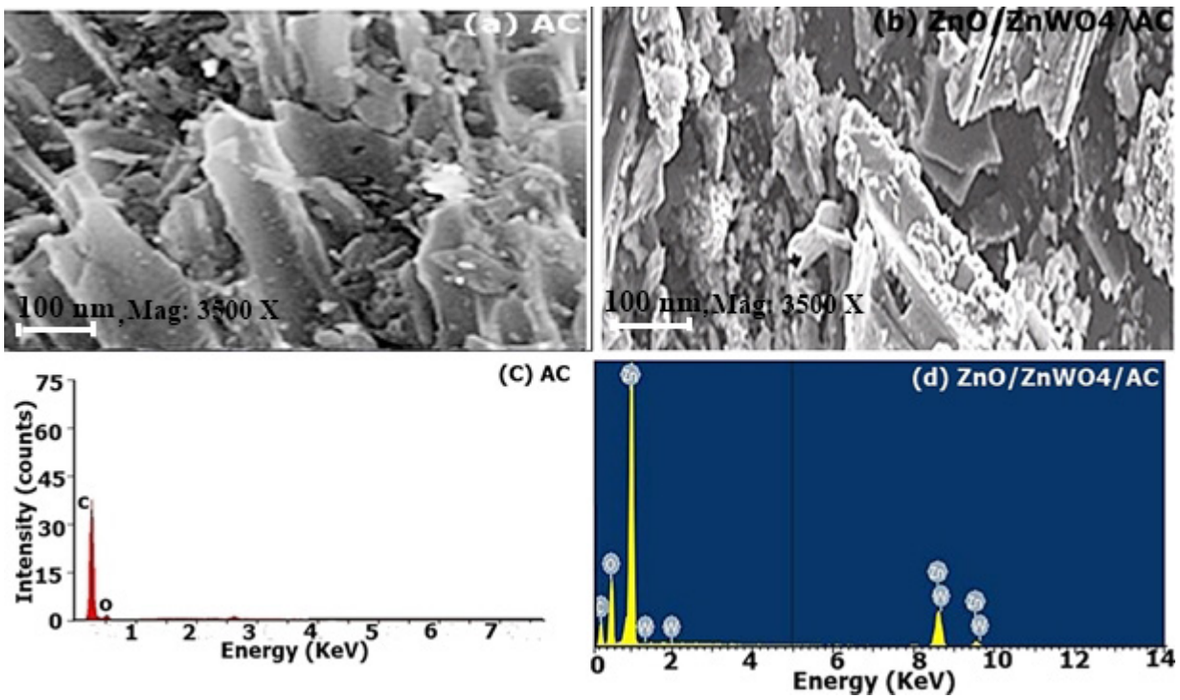

Fig. 1(a–d). SEM and EDX analysis of ZnO/$ZnWO_4$/AC. SEM images of (a) AC and (b) ZnO/$ZnWO_4$/AC. EDX images of (c) AC and (d) ZnO/$ZnWO_4$/AC.

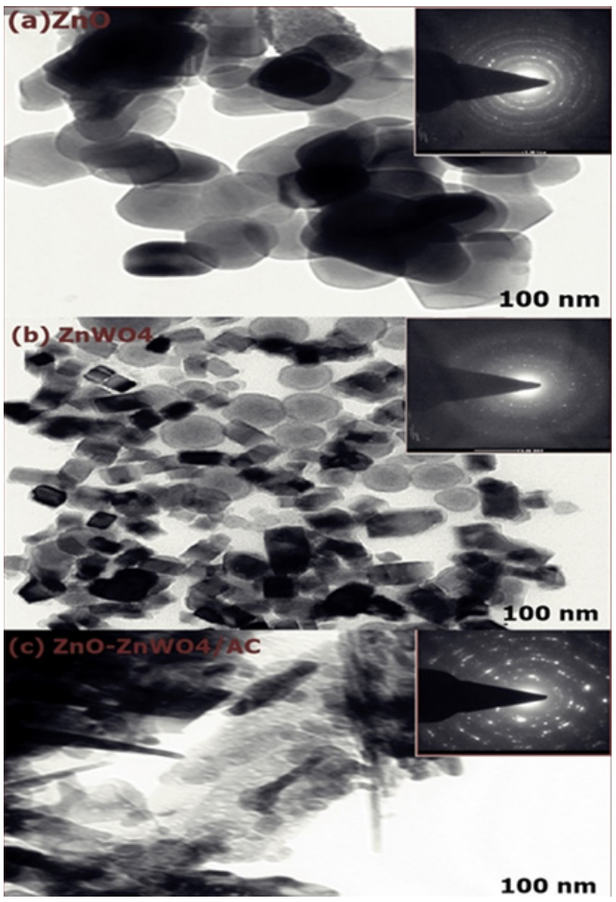

Fig. 2 (a–c). TEM images and SAED analysis of ZnO, $ZnWO_4$ and ZnO/$ZnWO_4$/AC. (a) TEM image of ZnO (Inset is SAED image of ZnO), (b) TEM image of $ZnWO_4$ (Inset is SAED image of $ZnWO_4$) and (c) TEM image of ZnO/$ZnWO_4$/AC (Inset is SAED image of ZnO/$ZnWO_4$/AC).

AC. The band at 1162 cm^{-1} was ascribed to C–O stretching vibration. Fig. 4b illustrates FTIR spectrum of $ZnWO_4$. The band at 592 cm^{-1} was ascribed to the bending vibrations of W–O group. The band at 798 cm^{-1} was assigned to stretching vibrations of W–O. The peaks at 874 cm^{-1} was referred to bending and stretching vibrations of Zn–O–W group in $ZnWO_4$ [23]. The peaks at 1384, 1628 and 3411 cm^{-1} were assigned to O–H stretching and O–H bending vibrations modes [24]. The bands at 2877 and 2985 cm^{-1} were due to C–O vibrations of CO_2 in atmosphere [25]. Fig. 4 (c) illustrates IR spectra of ZnO/$ZnWO_4$/AC nanocomposites. The peaks at 3415 and 1563 cm^{-1} were corresponded to hydroxyl groups [26,27]. The peak at observed at 3415 cm^{-1} was originated due to the O–H stretching vibrations of water present in ZnO and/or AC functional group [22]. The peak at 1334 cm^{-1} was assigned to deformation vibration of hydroxyl groups. The bands at 849 cm^{-1} was assigned to symmetrical stretching vibrations of the bridged oxygen atom in Zn–O–W. The absorption peaks at 440 cm^{-1} was due to W–O stretching mode in WO_6 [28,29].

The band gap of photocatalysts was determined using Tauc relation in Eq. (3) [30].

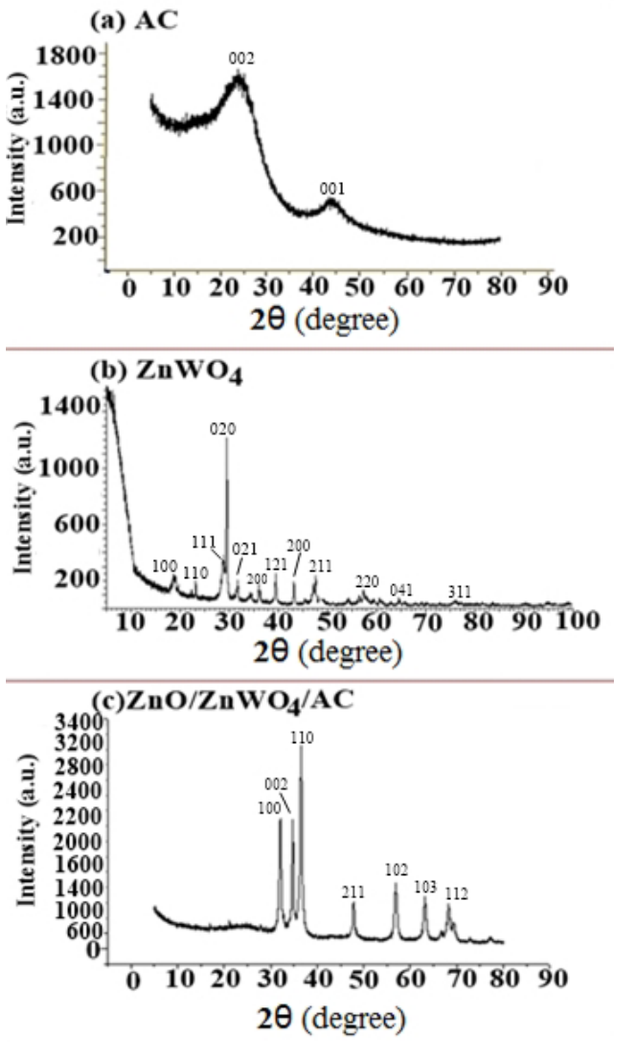

Fig. 3(a–c). XRD analysis of (a) AC, (b) $ZnWO_4$ and (c) ZnO/$ZnWO_4$/AC.

$$\alpha h\nu = B\left(h\nu - E_g\right)^n \tag{3}$$

where α = absorption coefficient = 2.303 A/l, E_g= optical band gap, B = band tailing parameter, hυ represents the photon energy and n = ½ for direct band gap. The optical band gap is determined by extrapolating the straight portion of curve between $(\alpha h\upsilon)^2$ and hυ when α = 0. The band gap of ZnO, $ZnWO_4$ and ZnO/$ZnWO_4$/AC was found to be 3.1, 3.39 and 3.32 eV, respectively (Fig. 5a). The pH_{zpc} of AC and ZnO/$ZnWO_4$/AC was calculated as 5.9 and 6.1 as respectively, (Figs. 5b and c).

3.2. AMP and OTC removal under different catalytic systems

Table 1 illustrates AMP and OTC removal under different catalytic systems. The photolysis in the absence of catalyst had no effect on AMP and OTC removal from

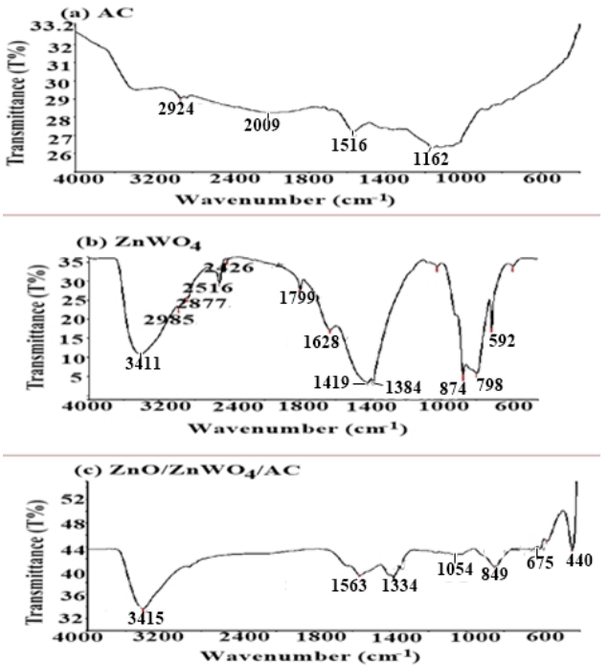

Fig. 4 (a–c). FTIR analysis of (a) AC, (b) $ZnWO_4$ and (c) ZnO/$ZnWO_4$/AC.

aqueous phase. 93%, 75%, 44%, 40% and 27% of removal efficiency was achieved utilizing ZnO/$ZnWO_4$/AC,ZnO/$ZnWO_4$, $ZnWO_4$, ZnO and AC respectively. However, in dark, ZnO/$ZnWO_4$/AC, ZnO/$ZnWO_4$, $ZnWO_4$, ZnO and AC exhibited 35%, 12%, 9%, 10%, and 25% of AMP removal from reaction solution (Table 1). In case of OTC, 96% and 70% of antibiotic was removed under solar light in 120 min using ZnO/$ZnWO_4$/AC, ZnO/$ZnWO_4$ respectively. While in the absence of solar light, 34% and 32% of removal efficiency was attained for ZnO/$ZnWO_4$/AC and AC respectively. Efficiency trend followed by adsorbents was: ZnO/$ZnWO_4$/AC ≈ AC < ZnO/$ZnWO_4$ < ZnO. The obtained trends indicates that the photocatalytic activity of ZnO/$ZnWO_4$/AC was entirely different from binary/ternary inorganic metal oxide photocatalyst. The adsorption behaviour of ZnO/$ZnWO_4$/AC was also explored for antibiotic removal.

3.3. Adsorption kinetics of ZnO/$ZnWO_4$/AC, ZnO/$ZnWO_4$ and AC

The amount of OTC/AMP adsorbed onto ZnO/$ZnWO_4$/AC, ZnO/$ZnWO_4$, AC at time t (min) was calculated using following equation [31,32]:

$$q_e = (C_o - C_e)\frac{V}{M} \quad (4)$$

Where q_e(mg g^{-1}) is the amount of AMP/OTC per gram of adsorbent at time t (min), C_0 is the initial concentration of antibiotics (dm^{-3}), C_t is the concentration of antibiotics (mol dm^{-3}) at time t (min), V denotes volume of reaction solution

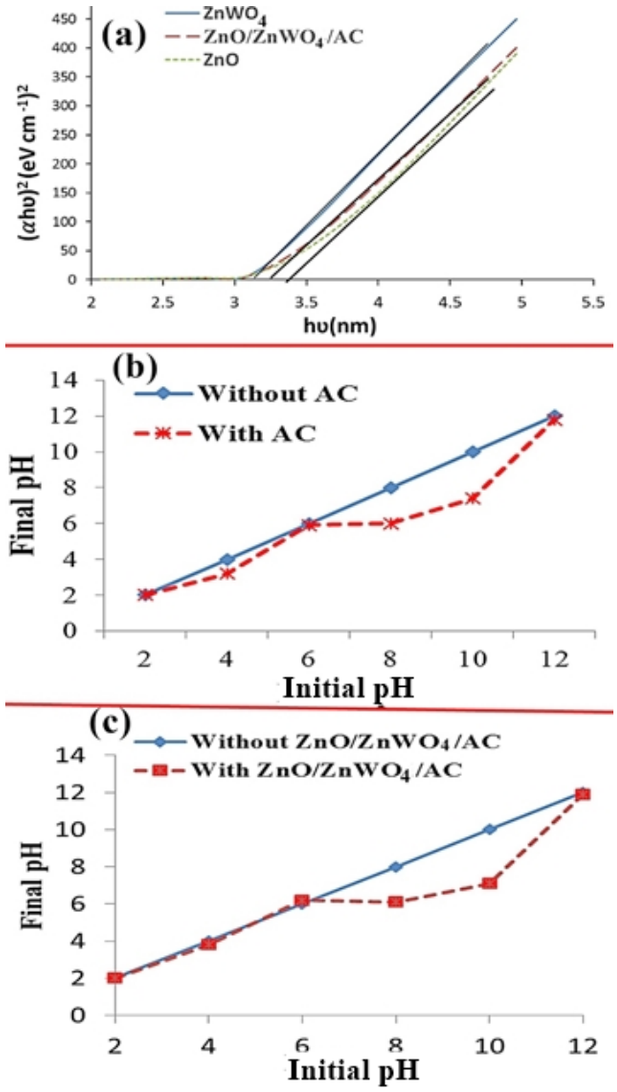

Fig. 5 (a–c). UV-visible analysis and pH_{zpc} analysis. (a) UV-visible reflectance spectra of ZnO, $ZnWO_4$ and ZnO/$ZnWO_4$/AC, (b) pH_{zpc} analysis of AC. (d) pH_{zpc} analysis of ZnO/$ZnWO_4$/AC.

Table 1
Photocatalytic and adsorptional removal of OTC and AMP using different catalytic systems: Reaction condition [AMP] = 1×10^{-4} mol dm^{-3}; [OTC] = 1×10^{-4} mol dm^{-3}; [catalyst] = 50 mg/100 ml; pH = 6.0; time = 60 min (AMP) and 120 min (OTC); Solar light intensity = $35 \times 10^3 \pm 1000$ lx

Catalytic system	% AMP removal		% OTC removal	
	Under solar light	In Dark	Under solar light	In Dark
ZnO/$ZnWO_4$/AC	93	35	96	34
ZnO/$ZnWO_4$	75	12	70	13
AC	27	25	24	32
ZnO	40	10	41	9
$ZnWO_4$	44	9	46	7

(50 ml) and m denotes the mass of the adsorbent (g). The pseudo first order rate is represented as Eq.(5) [31,32]:

$$\left(q_e - q_t\right) = \log q_e - \frac{k_1 t}{2.303} \tag{5}$$

where q_e and q_t are the amount of antibiotics adsorbed per gram of adsorbent at equilibrium and time t(mg/g). k_1 is first order rate constant (min^{-1}). The pseudo second order rate expression can be represented using Eq. (6) and (7) [31,32]:

$$\frac{q_t}{dt} = k_2\left(q_e - q_e\right)^2 \tag{6}$$

$$\frac{t}{q_t} = \frac{1}{k_1 q_e^2} + \frac{t}{q_e} \tag{7}$$

where q_e is the amount of OTC/AMP adsorbed per gram of adsorbent at equilibrium (mg/g), q_t describes the amount of adsorbate adsorbed at contact time t and k_2 is pseudo second order constant (g/mg min). The parameter q_e and k_2 can be estimated using a plot between t/q_t.

The kinetic data for antibiotics adsorption onto adsorbents is presented in Table 2. The value of correlation coefficient for second order was higher than first order kinetics. The adsorption of AMP and OTC obeyed pseudo second order kinetics. These studies revealed increased the adsorption capacity of the ZnO/$ZnWO_4$/AC as compared ZnO/$ZnWO_4$. The pH of an aqueous solution has significant effect on the adsorption of aqueous phase pollutants. At neutral pH, OTC is found as a H_2OTC and $HOTC^-$ where as AMP exits as $HAMP^-$ at near neutral and slightly basic pH. The pH of zero point charge (pH_{zpc}) of ZnO/$ZnWO_4$/AC and AC was found to be 6.1 and 5.9. Above pH_{zpc}, surface of ZnO/$ZnWO_4$/AC was predominantly negatively charged. While below pH_{zpc}, the surface of ZnO/$ZnWO_4$/AC and AC had positive charge [34]. At lower pH, both absorbent and OTC/AMP were positively charged and hence the adsorption of both the antibiotic was retarded [34,35]. However, both ZnO/$ZnWO_4$/AC and AC had positively charged surface below neutral pH. The negatively charged species of antibiotics were attracted towards positively charged absorbent molecules [34,35]. This caused higher adsorption of antibiotics onto adsorbent at pH 6 (Table 3). The decrease in adsorption at basic pH was due to negative charge on both absorbent and antibiotic molecules [34,35]. From the above discussion, we conclude that pH 6 was the optimal pH for the OTC and AMP adsorption onto the surface of ZnO/$ZnWO_4$/AC and AC. Langmuir-Hinshelwood model

Table 2
Adsorption kinetics for antibiotics adsorption onto absorbents. Reaction condition: [AMP] = 1×10^{-4} mol dm^{-3}; [OTC] = 1×10^{-4} mol dm^{-3}; [catalyst] = 50 mg/100 ml; pH = 6.0; reaction time = 120 min

	Pseudo first order kinetics					
	k_1 (min^{-1})		q_e (mg/g)		R^2	
	AMP	OTC	AMP	OTC	AMP	OTC
ZnO/$ZnWO_4$/AC	0.016	0.014	53.50	54.13	0.90	0.89
AC	0.014	0.013	51.56	50.00	0.92	0.91
ZnO/$ZnWO_4$	0.006	0.005	10.12	9.56	0.93	0.90
	Pseudo second order kinetics					
	k_2 (g/(mg min)		q_e (mg/g)		R^2	
	AMP	OTC	AMP	OTC	AMP	OTC
ZnO/$ZnWO_4$/AC	0.00012	0.00014	58.31	62.50	0.97	0.98
AC	0.0009	0.00013	57.22	59.00	0.98	0.97
ZnO/$ZnWO_4$	0.00004	0.00008	15.67	12.00	0.99	0.99

Table 3
Effect of pH on AMP and OTC adsorption. Reaction condition: [AMP] = 1×10^{-4} mol dm^{-3}; [OTC] = 1×10^{-4} mol dm^{-3}; [catalyst] = 50 mg/100 ml; pH = 6.0; reaction time = 120 min

Initial pH	AMP				OTC			
	ZnO/$ZnWO_4$/AC		ZnO/$ZnWO_4$		ZnO/$ZnWO_4$/AC		ZnO/$ZnWO_4$	
	q_e	Final pH	q_e	Final pH	q_e	Final pH	q_e	Final pH
2.0	14	1.9	16	1.9	21	1.9	12	1.8
4.0	22	2.5	20	3.7	45	2.7	37	3.5
6.0	60	5.7	60	6.2	64	5.5	63	5.9
8.0	38	7.2	34	6.6	47	6.9	22	6.9
10.0	17	9.2	16	8.8	22	8.5	9	8.1

claims that photodegradation of many organic compounds is a surface phenomenon [36]. In our case, the antibiotic degradation was negligible in the absence of catalyst. Further studies were undertaken to investigate the effect of adsorption antibiotics degradation.

3.4. Influence of adsorption on photodegradation of AMP and OTC

Figs. 6a and b show the removal efficiency of ZnO/$ZnWO_4$/AC, ZnO/$ZnWO_4$ and AC as function of time. The first portion of graph depicts the adsorption of AMP and OTC using various adsorbents. 35%, 12% and 25% of AMP removal was observed for ZnO/$ZnWO_4$/AC, ZnO/$ZnWO_4$ and AC respectively in 60 min. In case of OTC adsorption, 34%, 13% and 32% of removal efficiency was calculated for ZnO/$ZnWO_4$/AC, ZnO/$ZnWO_4$ and AC, respectively. During adsorption followed by catalysis (A-P), 52%, 40% and 27% of AMP was removed using ZnO/$ZnWO_4$/AC, ZnO/$ZnWO_4$ and AC in 120 min. The OTC removal efficiency for ZnO/$ZnWO_4$/AC, ZnO/$ZnWO_4$ and AC was found to be 56%, 40% and 33% respectively. During A-P, the decrease in effective photoactive volume was due to screening of solar light by adsorbed antibiotics. 93%, 75% and 27% of AMP was degraded using ZnO/$ZnWO_4$/AC, ZnO/$ZnWO_4$ and AC photocatalyst, respectively during simultaneous adsorption and photocatalysis (A+P) process. While 96%, 72% and 32% of OTC was removed for ZnO/$ZnWO_4$/AC, ZnO/$ZnWO_4$ and AC photocatalyst, respectively.

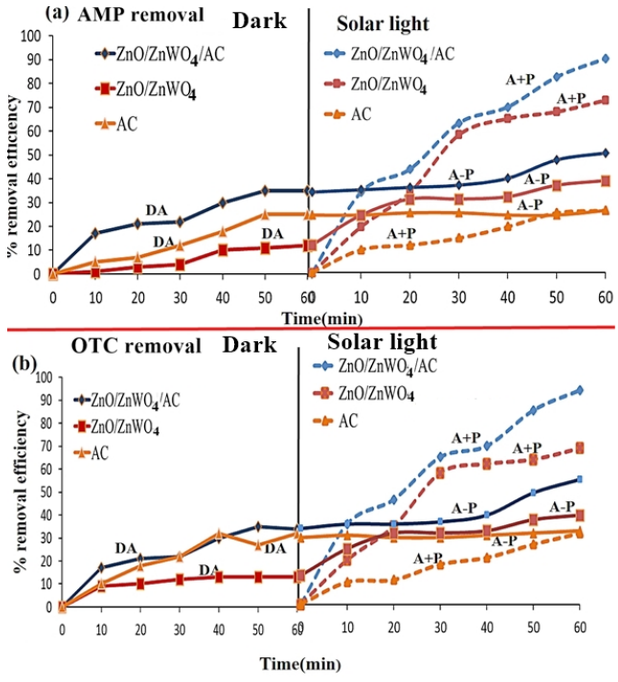

Fig. 6 (a and b). AMP (a) and OTC (b) removal using AC, ZnO/$ZnWO_4$ and ZnO/$ZnWO_4$/AC Reaction condition: [AMP] = 1 × 10^{-4} mol dm^{-3}; [OTC] = 1 × 10^{-4} mol dm^{-3}; [catalyst] = 50 mg/100 ml; pH = 6.0; Solar light intensity = 35 × 10^3 ± 1000 lx; reaction time = 120 min for DA and A-P and 120 min for A+P (OTC removal), 60 min for DA and A-P and 120 min for A+P (for AMP removal).

During A+P process, adsorbed antibiotics were instantaneously photo degraded by photocatalysts. ZnO/$ZnWO_4$/AC/A+P catalytic system was most efficient for AMP and OTC degradation. ZnO/$ZnWO_4$/AC/A+P catalytic system was most efficient due to beneficial combination of photocatalytic and adsorption process.

3.5. AMP and OTC mineralization kinetics using ZnO/$ZnWO_4$/A+P and ZnO/$ZnWO_4$/AC/A+P process

Langmuir-Hinshelwood model was used to explore the kinetics of AMP and OTC removal using ZnO/$ZnWO_4$/A+P and ZnO/$ZnWO_4$/AC/A+P process [37,38]: The plot between $-\ln(C/C_0)$ and time were plotted for AMP and OTC degradation. The value of rate constant was found to be 2.7 × 10^{-2} min^{-1} and 2.0 × 10^{-2} min^{-1} using ZnO/$ZnWO_4$ and ZnO/$ZnWO_4$/AC/A+P catalytic systems, respectively. The degradation process followed pseudo first order kinetics during initial hours of photodegradation process.

Now, antibiotics were exposed to solar light in presence of photocatalyst (A+P) for 10 h to obtain complete mineralization of antibiotics. The COD and CO_2 measured to investigate the extent of OTC and AMP mineralization (Figs. 6 a,b). During 8 h of exposure, 99% and 85% of COD removal was attained for AMP mineralisation using ZnO/$ZnWO_4$/AC and ZnO/$ZnWO_4$ respectively. While 70% and 60% of COD removal was obtained using ZnO/$ZnWO_4$/AC and ZnO/$ZnWO_4$ respectively. The CO_2 formation during mineralization process also specified the completion of mineralization process. Furthermore, the formation of NO_3^- and SO_4^{2-} ions during degradation of antibiotics established the mineralization of AMP and OTC.

The power law model was used to understand the kinetics of OTC and AMP degradation during mineralization process using ZnO/$ZnWO_4$/AC/A+P and ZnO/$ZnWO_4$/A+P catalytic systems Eq. (8) [38]:

$$R = k_1 [ANT]^{n1} \tag{8}$$

where k_1 is rate constant for photocatalysis and n_1 denotes the order of the reaction for photocatalysis. Figs. 7c–f present the goodness of fit of rate Eq. (8). The obtained results are given in Table 4. For AMP degradation, order of reaction (n_1) was given by 1.56 and 1.88 for ZnO/$ZnWO_4$/AC/A+P and ZnO/$ZnWO_4$/A+P catalytic systems respectively. The catalytic systems ZnO/$ZnWO_4$/AC/A+P and ZnO/$ZnWO_4$/A+P had respective rate constants of 8.17 × 10^{-8} (mol dm^{-3})$^{-0.56}$ h^{-1} and 3.19 × 10^{-8} (mol dm^{-3})$^{-0.88}$ h^{-1} (Table 4). For OTC removal, the order of reaction was calculated as 1.54 and 1.69 for ZnO/$ZnWO_4$/AC/A+P and ZnO/$ZnWO_4$/A+P catalytic processes, respectively. The rate constant for ZnO/$ZnWO_4$/AC/A+P and ZnO/$ZnWO_4$/A+P catalytic processes was given by 8.67 × 10^{-8} (mol dm^{-3})$^{-0.54}$ h^{-1} and 4.7 × 10^{-8} (mol dm^{-3})$^{-0.69}$ h^{-1}, respectively. The order of reaction more than one signifies the complex nature of degradation process. The degradation process tends to slow with the increase in degradation time and overall process of mineralization is complicated in nature.

During heterogeneous photodegradation, hydroxyl radicals with oxidation potential of 2.8 eV are regarded as main oxidizing agent [39]. To examine the role of OH· during photodegradation process, degradation experi-

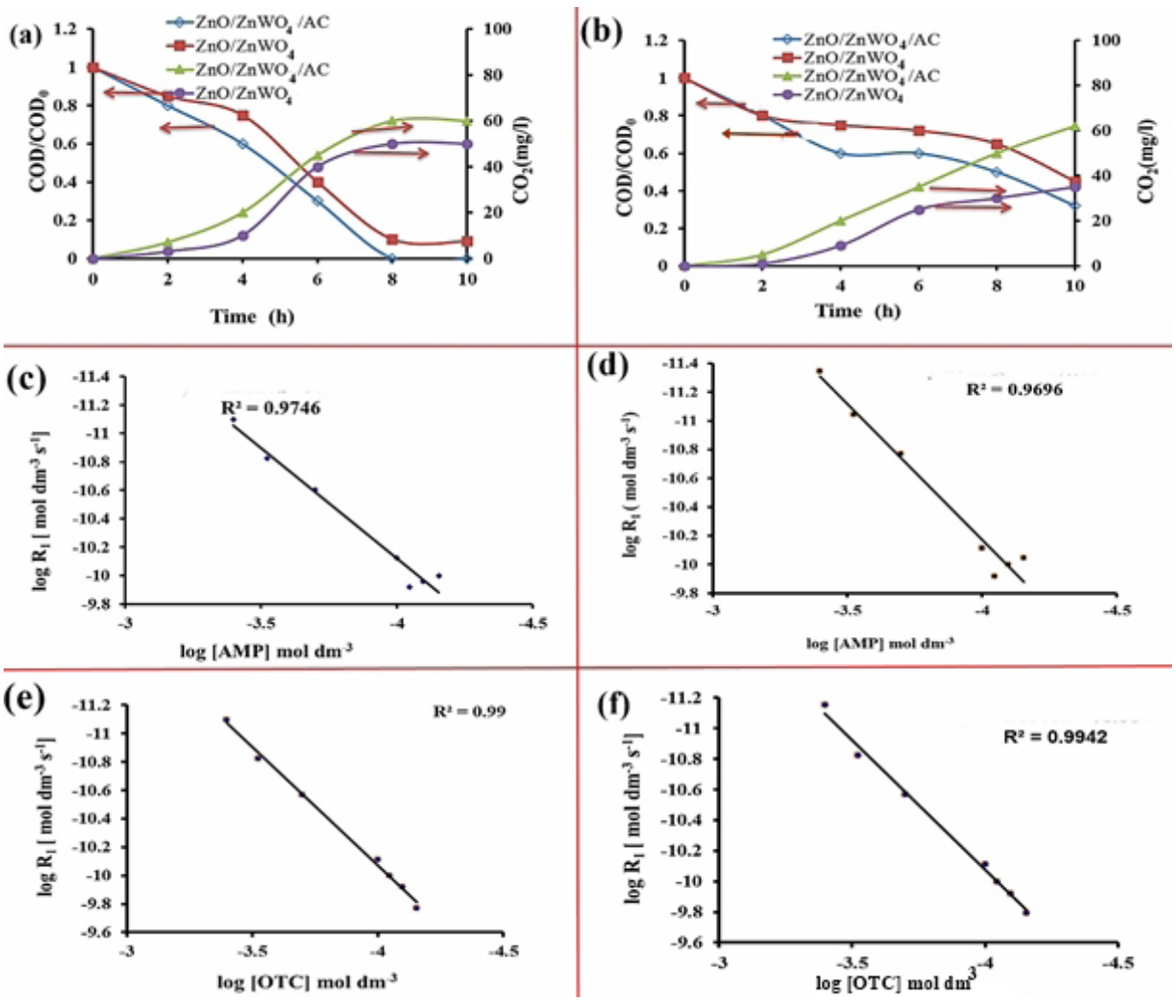

Fig. 7 (a and b). Mineralization kinetics of OTC and AMP. COD and CO_2 measurements during mineralization AMP of (Fig. 7a) and OTC of (Fig. 7b). Reaction conditions: [AMP] = 1 × 10^{-4} mol dm^{-3}; [OTC] = 1 × 10^{-4} mol dm^{-3}; [catalyst] = 50 mg/100 ml ; pH = 6.0; Solar light intensity = 35 x 10^3 ± 1000 lx; reaction time = 10 h.

Table 4
Kinetic parameter for mineralization of OTC and AMP. Reaction parameter: [catalyst] = 50 mg/100 ml; pH = 6.0; Solar light intensity = 35 × 10^3 ± 1000 lx; reaction time = 10 h

Parameters	$ZnO/ZnWO_4$/AC/ A+P	$ZnO/ZnWO_4$/A+P
[a]n_1	1.56	1.88
[a]k_1	8.17 × 10^{-8} (mol dm^{-3})$^{-0.56}$ h^{-1}	3.19 × 10^{-8} (mol dm^{-3})$^{-0.88}$ h^{-1}
[a]R	8.17 × 10^{-8} [AMP]$^{1.56}$mol dm^{-3} h^{-1}	3.19 × 10^{-8} [AMP]$^{1.88}$ mol dm^{-3} h^{-1}
[b]n_1	1.54	1.69
[b]k_1	8.67 × 10^{-8} (mol dm^{-3})$^{-0.54}$ h^{-1}	4.7 × 10^{-8} (mol dm^{-3})$^{-0.69}$ h^{-1}
[b]R	8.67 × 10^{-8} [OTC]$^{1.54}$ mol dm^{-3} h^{-1}	4.7 × 10^{-8} [OTC]$^{1.69}$ mol dm^{-3} h^{-1}

The superscript "a" means AMP and "b" means OTC.

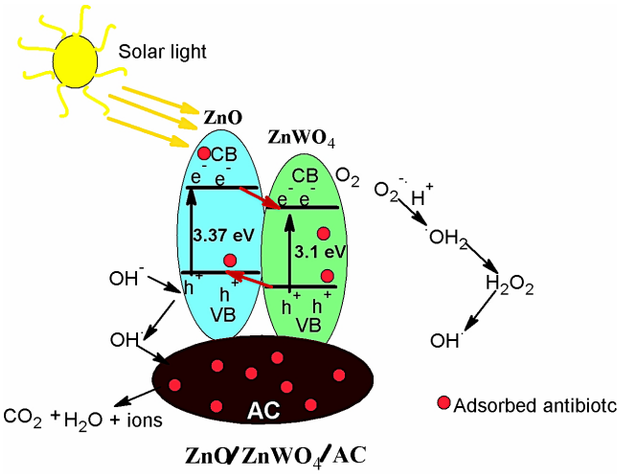

Fig. 8. Mechanistic view of photocatalytic antibiotic mineralization using $ZnO/ZnWO_4$/AC.

ments were performed with hydroxyl radical scavenger, isopropanol. A high second order rate constant (6×10^9 M^{-1} S^{-1}) of isopropanol with hydroxyl radical was reported by Buxton and co-workers [40]. The removal efficiency of AMP and OTC was reduced to 9% and 7%, respectively for ZnO/$ZnWO_4$/AC/A+P process in the presence of isopropanol. The reduction in removal efficiency in the presence of holes (NaCl) and oxygen scavenger (tertiary butyl alcohol) was very minor [37,41]. So, we concluded that OTC and AMP degradation occurred mainly via hydroxyl radical assisted process.

In ZnO/$ZnWO_4$/AC heterostructure, photo-generated electron can easily transfer from more negative potential of conduction band to more positive potential of conduction band of a semiconductor. While holes migrate from more positive potential of valence band to the less positive potential of valence band of a semiconductor. These migration of electron-hole pair in opposite direction strongly prevent the rate of recombination [17]. The efficient charge separation increases the lifetime of charge carriers and enhance the transfer of interfacial charge to adsorbed species. The conduction band electrons form OH· with O_2. The valance band electrons reacted with H^+/H_2O to form OH·. Finally, OH· mineralized OTC and AMP into CO_2 and ions. The higher adsorption rate and degradation of OTC and AMP was due to presence of activated carbon present in ZnO/$ZnWO_4$/AC. In the meantime, the adsorbed OTC or AMP was mineralized during A+P process.

The recycle efficiency of a photocatalyst is a key factor for real time applicability of the process. Both ZnO/$ZnWO_4$/AC and ZnO/$ZnWO_4$ were separated from reaction solution via centrifugation process. For AMP removal, the removal efficiency of ZnO/$ZnWO_4$/AC was reduced to 88% from 93% as shown in Fig. 9a, whereas removal efficiency of ZnO/$ZnWO_4$ had a decrease from 75% to 65%. During OTC removal after ten successive catalytic cycles, the removal efficiency of ZnO/$ZnWO_4$/AC and ZnO/$ZnWO_4$ was found to be 91% and 60% respectively in Fig.9b.

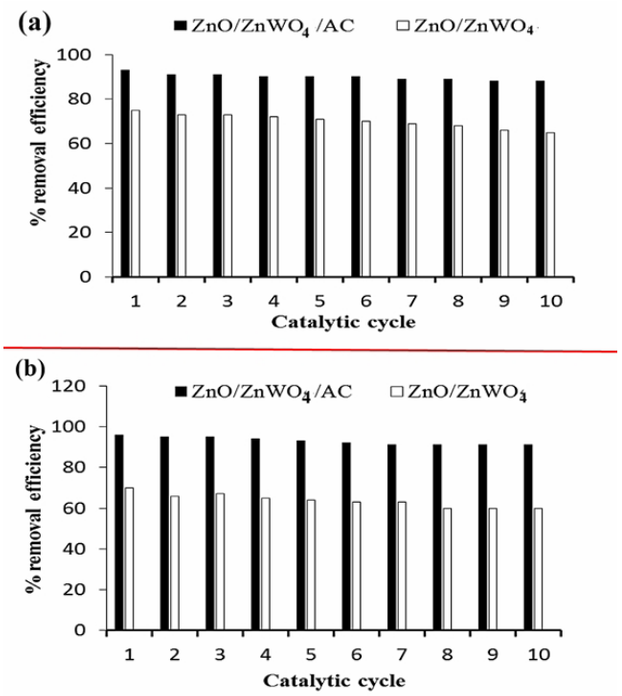

Fig. 9. Recycle efficiency of ZnO/$ZnWO_4$/AC and ZnO/$ZnWO_4$. Reaction conditions: [AMP] = 1×10^{-4} mol dm^{-3} ; [OTC] = 1×10^{-4} mol dm^{-3} ; [catalyst] = 50 mg/100 ml ; pH = 6.0; Solar light intensity = $35 \times 10^3 \pm 1000$ lx; reaction time = 10 h.

4. Conclusion

In summary, ZnO/$ZnWO_4$ was supported onto activated carbon (AC) to overcome the limitations such recombination, agglomeration and separation of photocatalyst from reaction solution. The various spectral techniques FESEM, TEM, FTIR, XRD, EDX, BET and UV-visible diffuse reflectance confirmed the successful formation of ZnO/$ZnWO_4$/AC. The optical band gap of ZnO/$ZnWO_4$/AC was found to be 3.32 eV. The semicrystalline nature of ZnO/$ZnWO_4$/AC was revealed by XRD analysis. The pH of zero point charge (pH_{zpc})of ZnO/$ZnWO_4$/AC was obtained as 6.1.ZnO/$ZnWO_4$/AC displayed substantial adsorption capacity for AMP and OTC removal. The adsorption of antibiotics followed the pseudo second order kinetics. Furthermore, adsorption had positive effect on the photocatalytic degradation of ampicillin and oxytetracycline. During A-P process, the adsorption of antibiotics reduced the photodegradation process. While in A+P process, synergistic effect between adsorption and photocatalysis was observed. The complete mineralization of AMP about 99% was attained in 8 h using ZnO/$ZnWO_4$/AC/A+P catalytic system. In case of OTC, only 70% of antibiotic was mineralized to CO_2, H_2O and NO_3^- ions in 8 h. The mineralization was a slower and challenging process compared to degradation process. According to precedent work, activated carbon supported ZnO/$ZnWO_4$ can be used as both an adsorbent and photocatalyst for treatment of wastewater that contains OTC and AMP. The supported photocatalyst is more advantageous due to the easy separation and reusability.

References:

[1] P. Raizada, P. Singh, A. Kumar, B. Pare, S.B. Jonnalagadda, Preparation and photocatalytic activity of hydroxyapatite supported BiOCl nanocomposite for oxytetracycline removal, Adv. Mater. Lett., 7 (2016) 312–318.
[2] B. Priya, P. Shandilya, P. Raizada, P. Thakur, N. Singh, P. Singh, Photocatalytic mineralization and degradation kinetics of ampicillin and oxytetracycline antibiotics using graphene sand composite and chitosan supported BiOCl, J. Mol. Cat. A, 423 (2016) 400–413.
[3] P. Raizada, P. Singh, A. Kumar, B. Pare, S.B. Jonnalagadda, Zero valent iron-brick grain nanocomposite for enhanced solar-Fenton removal of malachite green, Sep. Purif. Technol., 133 (2014) 429–437.
[4] J. Esmaili-Hafshejani, A. Nezamzadeh-Ejhieh, Increased photocatalytic activity of Zn(II)/Cu(II) oxides and sulfides by coupling and supporting them onto clinoptilolite nanoparticles in the degradation of benzophenone aqueous solution, J. Hazard. Mater., 316 (2016) 194–203.
[5] A. Nezamzadeh-Ejhieh, M. Bahrami, Investigation of the photocatalytic activity of supported ZnO–TiO_2 on clinoptilolite nano-particles towards photodegradation of wastewater-contained phenol, Desal. Water Treat., 55 (2015) 1096–1104

[6] P. Raizada, P. Singh, A. Kumar, G. Sharma, B. Pare, S.B. Jonnalagadda, P. Thakur, Solar photocatalytic activity of nano-ZnO supported on activated carbon or brick grain particles, role of adsorption in dye degradation, Appl. Catal. A., 486 (2014) 159–169.
[7] W.W. Lee, W.H. Chung, C.S. Lu, W.Y. Lin, C. Chen, A study on the degradation efficiency and mechanisms of ethyl violet by HPLC–PDA–ESI–MS and GC–MS, Sep. Purif. Technol., 98 (2012) 488–496.
[8] P. Singh, P. Raizada, D. Pathania, A. Kumar, P. Thakur, Preparation of BSA-$ZnWO_4$ nanocomposites with enhanced adsorptional photocatalytic activity for methylene blue degradation, Int. J. Photoenergy, 2013 (2013) 7.
[9] M.J. Kim, Y.D. Huh, Ligand-assisted hydrothermal synthesis of $ZnWO_4$ rods and their photocatalytic activities, Mater. Res. Bull., 45 (2010) 1921–1924.
[10] W. Zhao, X. Song, G. Chen, S. Sun, One-step template-free synthesis of $ZnWO_4$ hollow clusters, J. Mater. Sci., 44 (2009) 3082–3087.
[11] J. Bi, L. Wu, Z. Li, Z. Li, Z. Ding, X. Wang, X. Fu, A facile microwave solvothermal process to synthesize $ZnWO_4$ nanoparticles, J. Alloys Compd., 480 (2009) 684–688.
[12] S. Lin, J. Chen, X. Weng, L. Yang, X. Chen, Fabrication and photocatalysis of mesoporous $ZnWO_4$ with PAMAM as a template, Mater. Res. Bull., 44 (2009) 1102–1105.
[13] T. Montini, V. Gombac, A. Hameed, L. Felisari, G. Adami, P. Fornasiero, Synthesis, characterization and photocatalytic performance of transition metal tungstates, Chem. Phys. Lett., 498 (2010) 113–119.
[14] Y. Zhu, Li. Wang, Visible photocatalytic activity enhancement of $ZnWO_4$ by graphene hybridization, ACS Catal., 2 (2012) 2769–2778.
[15] S. Gautam, P. Shandilya, B. Priya, V.P. Singh, P. Raizada, R.S. Rai, M.A. Valente, P Singh, Superparamagnetic $MnFe_2O_4$ dispersed over graphitic carbon sand composite and bentonite as magnetically recoverable photocatalyst for antibiotic mineralization, Sep. Purif. Technol., 172 (2017) 498–511.
[16] P. Raizada, P. Singh, P. Thakur, Solar light induced photodegradation of oxytetracycline using Zr doped TiO_2/CaO based nanocomposite, Indian J. Chem., 55A (2016) 803–809.
[17] H. Derikvandi, A. Nezamzadeh-Ejhieh, Increased photocatalytic activity of NiO and ZnO in photodegradation of a model drug aqueous solution: Effect of coupling, supporting, particles size and calcination temperature, J. Hazard. Mater., 321 (2017) 629–638.
[18] A.R. Phani, M. Passacantando, L. Lozzi, S. Santucci, Structural characterization of bulk $ZnWO_4$ prepared by solid state method, J. Mater. Sci., 35 (2000) 4879–4883.
[19] Q. Huang, X. Wang, J. Li, C. Dai, S. Gamboa, P.J. Sebastian, Nickel hydroxide/activated carbon composite electrodes for electrochemical capacitors, J. Power Sources, 164 (2007) 425–429.
[20] D. Jamwal, G. Kaur, P. Raizada, P. Singh, D. Pathak, P. Thakur, Twin-tail surfactant peculiarity in superficial fabrication of semiconductor quantum dots: toward structural, optical, and electrical features. J Phys. Chem. C, 119 (2015) 5062–5073.
[21] S. Komarneni, R. Roy, Q.H. Li, Microwave-hydrothermal synthesis of ceramic powders, Mater. Res. Bull., 27 (1992) 1393–1405.
[22] H.D. Xie, D.Z. Shen, X.Q. Wang, G.Q. Shen, Growth and characterization of $KBi(WO_4)_2$ single crystals. Cryst. Res. Technol., 42 (2007) 18–22.
[23] A. Kumar, I. Xagoraraki, Pharmaceuticals, personal care products and endocrine-disrupting chemicals in U.S. surface and finished drinking waters: A proposed ranking system, Sci. Total Environ., 408 (2010) 5972–5989.
[24] M. Gotic, M. Ivanda, S. Popovic, Synthesis of nano crystalline iron oxide particles in the iron (III) acetate/alcohol/acetic acid system, Mater. Sci. Eng. B., 7 (2000) 193.
[25] H.D. Xie, D.Z. Shen, X.Q. Wang, G.Q. Shen, Kinetics of photocatalytic mineralization of oxytetracycline and ampicillin using activated carbon supported ZnO/$ZnWO_4$ nanocomposite in simulated wastewater, Cryst. Res. Technol., 42 (2007) 18–22.
[26] R.P. Jia, G.X. Zhang, Q.S. Wu, Y.P. Ding, $ZnWO_4$–TiO_2 composite nanofilms: preparation, morphology, structure and photoluminescent enhancement, Mater. Lett., 61 (2007) 1793–1797.
[27] A. Dodd, A. Mckinley, T. Tsuzuki, M. Saunders, Mechanochemical synthesis of nanoparticulate ZnO–$ZnWO_4$ powders and their photocatalytic activity, J. Eur. Cera. Soc., 29 (2009) 139–144.
[28] B. Pare, P. Singh, S.B. Jonnalagadda, Degradation and mineralization of Victoria blue B dye in a slurry photoreactor using advanced oxidation process, J. Sci. Indus. Res., 68 (2009) 724.
[29] P. Kulshrestha, R.F. Giese, D.S. Aga, Investigating the molecular interactions of oxytetracycline in clay and organic matter: Insights on factors affecting its mobility in soil, Environ. Sci. Technol., 38 (2004) 4097.
[30] B. Priya, P. Raizada, N. Singh, P. Thakur, P. Singh, Adsorptional photocatalytic mineralization of oxytetracycline and ampicillin antibiotics using Bi_2O_3/BiOCl supported on graphene sand composite and chitosan, J. Colloid Interf. Sci., (2016) 271–283.
[31] V.K. Gupta, D. Pathania, S. Sharma, P. Singh, Preparation of bio-based porous carbon by microwave assisted phosphoric acid activation and its use for adsorption of Cr (VI), J. Colloid. Interface. Sci., 401 (2013) 125–132.
[32] P. Singh, P. Raizada, D. Pathania, G. Sharma, P. Sharma, Microwave induced KOH activation of guava peel carbon as an adsorbent for congo red dye removal from aqueous phase, Indian. J. Chem. Technol., 20 (2013) 305–311.
[33] C. Zhao, M. Pelaez, X. Duan, H. Deng, K. O'Shea, D. Fatta-Kassinos, D.D. Dionysiou, Role of pH on photolytic and photocatalytic degradation of antibiotic Oxytetracycline in aqueous solution under visible/solar light: Kinetics and mechanism studies, Appl. Catal. B Environ., 134–135 (2013) 83–92.
[34] M.A. Anaraki, A. Nezamzadeh-Ejhieh, Modification of an Iranian clinoptilolite nano-particles by hexadecyltrimethyl ammonium cationic surfactant and dithizone for removal of Pb(II) from aqueous solution, J. Colloid Interface Sci., 440 (2015) 272–281.
[35] E.S. Elmolla, M. Chaudhuri, Degradation of amoxicillin, ampicillin and cloxacillin antibiotics in aqueous solution by the UV/ZnO photocatalytic process, J. Hazard. Mater., 173 (2010) 445–449.
[36] D. Dimitrakopoulou, I. Rethemiotaki, Z. Frontistis, N.P. Xekoukoulotakis, D. Venieri, D. Mantzavinos, Degradation, mineralization and antibiotic inactivation of amoxicillin by UV-A/TiO_2 photocatalysis, J. Environ. Manage., 98 (2012) 168–174.
[37] B. Pare, P. Singh, S.B. Jonnalgadda, Visible light induced heterogeneous advanced oxidation process to degrade pararosanilin dye in aqueous suspension of ZnO, Indian. J. Chem. Sect. A., 47 (2008) 830–835.
[38] J. Saien, R.R. Ardjmand, H. Iloukhani, Photocatalytic decomposition of sodium dodecyl benzene sulfonate under aqueous media in the presence of TiO_2, Phys. Chem. Liq., 41 (2003) 519–531.
[39] S. Gautam, P Shandilya, V.P. Singh, P. Raizada, P. Singh, Solar photocatalytic mineralization of antibiotics using magnetically separable $NiFe_2O_4$ supported onto graphene sand composite and bentonite , J. Water Process. Eng., 20 (2013) 305–311, 581–590.
[40] G.V. Buxton, C. Greenstock, W.P. Hellman, A.B. Ross, Critical review of rate constants for reactions of hydrated electrons, hydrogen atoms and hydroxyl radicals (.OH/.O-) in aqueous solution, J. Phys. Chem. Ref., 17 (1988) 513–886.
[41]. B. Pare, S.B. Jonnalagadda, H. Tomar, P. Singh, V.W. Bhagwat, ZnO assisted photocatalytic degradation of acridine orange in aqueous solution using visible irradiation, Desalination, 232 (2008) 80–90.